Journal of Physics and Chemistry of Solids 124 (2019) 242–249

Contents lists available at ScienceDirect

Journal of Physics and Chemistry of Solids

journal homepage: www.elsevier.com/locate/jpcs

Modelling the contribution of semi-core electrons to the dielectric function

Maarten Vos[a,*], Pedro L. Grande[b]

[a] Electronics Materials Engineering, Research School of Physics and Engineering, The Australian National University, Canberra, 0200, Australia
[b] Ion Implantation Laboratory, Institute of Physics, Federal University of Rio Grande Do Sul, Av. Bento Gonçalves 9500, CP 15051, CEP 91501-970, Porto Alegre, RS, Brazil

ARTICLE INFO

Keywords:
Dielectric function
Semi-core levels
Stopping
Ionization

ABSTRACT

Many aspects of the interaction of charged particles with matter can be expressed in terms of the dielectric function $\varepsilon(q, \omega)$. The dielectric function is relatively well known in the optical limit ($q = 0$) but, for example, stopping power calculations require the knowledge of the dielectric function for $q \neq 0$. Several approaches have been used to extend the dielectric function to $q \neq 0$ for both the valence electrons, using variations of the Lindhard dielectric function and the core levels where an atomic description can be used. The intermediate case of shallow core levels is somewhat problematic. Here collective effects modify the atomic picture, and the hydrogenic approximation of the wave function is less accurate. In this paper we describe a new extension scheme of the contribution to the energy loss function of shallow core levels to $q \neq 0$ and show that tor Al and Si it describes the experimental stopping data somewhat better than previous approaches. It also describes reasonably well the proton and electron induced ionization cross section of these shallow core levels. Lastly we investigate the dielectric function in the limit of high momentum, where it can be interpreted as a Compton profile. An approximation scheme in terms of Mermin dielectric function with an amplitude that depends on q works in all cases quite well.

1. Introduction

Describing the interaction of charged particles with matter is of great importance for a variety of fields ranging from materials science [1] to medical physics [2]. This interaction can be conveniently described in terms of the energy (ω) and momentum (q)-dependent dielectric function: $\varepsilon(q, \omega)$ [3,4]. In order to calculate physical observables it is then required that the dielectric function is known over a large range of q and ω values. For many materials $\mathrm{Im}[-1/\varepsilon(q, \omega)]$ has been determined in the optical limit (at $q = 0$) [5], and this quantity is called energy loss function or ELF. Extension of the ELF in the otical limit over all q values is thus required for the calculation of quantities such as proton stopping, electron inelastic mean free path, and Compton profiles. (Sometimes, e.g. in the case of stopping in the high energy ('Bethe') limit contributions near $q = 0$ dominate and observables can be calculated from the knowledge of $\mathrm{Im}[-1/\varepsilon(q, \omega)]$ at $q = 0$, and some basic assumption on the dispersion e.g. Ref. [6].) If one can identify a certain part of the dielectric function with an electron shell, then it is also possible to calculate ionization probabilities for this shell if $\varepsilon(q, \omega)$ is known over a range of ω and q values.

The choice of possible dielectric functions is severely restricted by sum rules that should apply [7]. In particular the Bethe (or Thomas-Reiche-Kuhn) sum rule:

$$\frac{1}{2\pi^2}\int_0^\infty \omega \mathrm{Im}[-1/\varepsilon(\mathrm{q},\omega)]\mathrm{d}\omega = \mathrm{N}, \tag{1}$$

and the f sum rule:

$$\frac{1}{2\pi^2}\int_0^\infty \omega \mathrm{Im}[\varepsilon(\mathrm{q},\omega)]\mathrm{d}\omega = \mathrm{N}, \tag{2}$$

should apply for any q value, with N the number of electrons per unit volume. (We are using atomic units throughout.) Another important restriction is that the imaginary and real part of $\varepsilon(q, \omega)$ are Kramers-Kronig pairs:

$$\mathrm{Re}\left[\frac{1}{\varepsilon(\mathrm{q},\omega)}\right] - 1 = \frac{1}{\pi}\mathscr{P}\int_{-\infty}^{\infty} \mathrm{d}\omega' \frac{1}{\omega' - \omega}\mathrm{Im}\left[\frac{1}{\varepsilon(\mathrm{q},\omega')}\right], \tag{3}$$

where $\mathscr{P}$ indicates the Cauchy principal value. For $\omega, q = 0$ the left hand side of eq. (3) is equal to $1/n^2 - 1$ with n the static refractive index and then this equation is known for metals (where $1/n = 0$) as the perfect screening sum rule.

Extension to values $q \neq 0$ are, for the valence band, often based on the Drude-Lindhard [8–10], Lindhard [11] or the Mermin dielectric function [12]. The advantages and disadvantages of the various

* Corresponding author.
E-mail address: maarten.vos@anu.edu.au (M. Vos).

https://doi.org/10.1016/j.jpcs.2018.09.020
Received 11 July 2018; Received in revised form 11 September 2018; Accepted 14 September 2018
Available online 19 September 2018
0022-3697/

approaches have been summarized recently in a review by Nikjoo et al. [13]. Here we will explore the possibilities to use the Mermin dielectric function to model the ELF and in particular focus on a way to get a good description for the semi-core levels that contribute to the ELF for energy losses exceeding their binding energy, often with a well-defined, sharp onset. The sharp onset suggests that one has to truncate the Memin loss function at this energy, as was first done by Abril et al. [12]. Such a truncation, although convenient for fitting the ELF, causes a dependency on q of the electron density as obtained from the Bethe sum rule. Abril et al. suggested to solve this problem by making the truncation energy dependent on q. Here we will suggest an alternative way of dealing with this problem, and show that the alternative way leads to a better description of a number of observables.

2. Description of the ELF

The Lindhard (Mermin) loss function describes a free electron gas, and has one (two) parameter(s), the plasmon energy ω_i defined by the electron density N of the free electron gas: $\omega_i^2 = 4\pi N$ (and the relaxation broadening (Γ_i)). However, real solids are more complex and consists of areas of varying electron density. To overcome this problem Ritchie and Howie introduced the electron gas statistical model [14] (see also [11,15], where the solid is described as a sum of different volumes with their corresponding electron densities and the ELF is then approximated as a sum of ELF's of Mermin dielectric functions (or Drude-Lindhard dielectric functions, which coincide with Mermin dielectric function with the same parameters at $q = 0$) each with their own energy ω_i and width Γ_i and weight A_i. Here A_i is the fraction of the unit cell with electron density corresponding to ω_i.

The contribution of inner shell electrons, who retain largely their atomic character, is conveniently calculated using the Generalized Oscillator Strength (GOS) $df/d\omega(q, \omega)$ based on hydrogen-like wave function in combination with the concept of effective charge as introduced by Slater [16]. The relation of the GOS to the dielectric function is given by [17]:

$$\frac{df}{d\omega}(q, \omega) = \frac{2\omega}{\pi E_a^2}\mathrm{Im}\left[\frac{-1}{\varepsilon(q, \omega)}\right], \tag{4}$$

with $E_a^2 = 4\pi n_a$ (n_a the atomic density) i.e. the plasmon energy corresponding to one electron per atom. In Fig. 1 we show the calculated minimum excitation energy of this model and the actually observed core level energies.

For binding energies above 1000 eV the agreement is generally quite good, but for lower energies there are substantial differences. Here the hydrogenic approximation becomes poor and collective effects

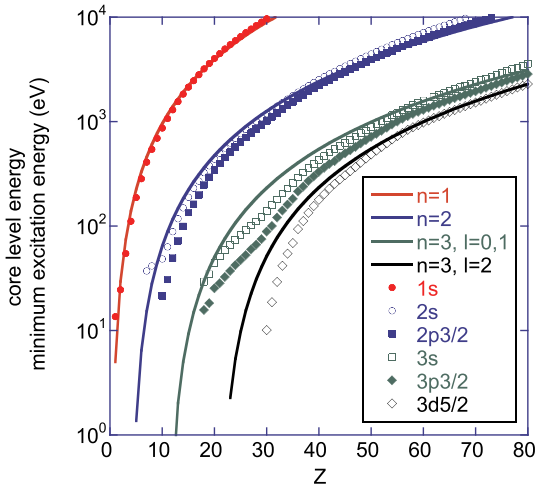

Fig. 1. The calculated minimum excitation energies for hydrogenic wave function (solid lines) versus the actually observed ones (symbols) [18].

may have significant influences. Modelling the observed dielectric function with the GOS of hydrogenic wave function does not reproduce the position of the sharp onset for these levels at $\varepsilon(0, \omega)$, or, if the formula is adjusted so the right onset position is obtained, result in a the wrong number of electrons in the shell. In addition, the GOS values for small q values and energy transfers between the actual edge and the minimum energy transfer in a hydrogen-like atom can be downright wrong (see e.g. the middle panel of Fig. 2 and Fig. 3).

Abril et al. found that it was possible to get a good description of the shape of the ELF of semi-core electrons using truncated Mermin functions, i.e. the Mermin loss function, above a certain energy loss, but put to zero at smaller losses [12]. Simply truncating the Mermin loss function at the same energy for all q values would cause different outcomes of the sum rule at different q values. Hence they made the truncation energy ω_{edge} a function of q, in such a way that the sum rule (eq. (1)) resulted in the same N values for all q. We will refer to this method as the $\omega_{\mathrm{edge}}(q)$ method. Here we want to explore as an alternative making A_i a function of q and refer to this way as the $A(q)$ method. $A_i(q)$ would then be determined so that at each q the sum rule (eq. (1)) corresponds to the same N value. In that case the contribution $A_i(q)$ has to be defined as:

$$\mathrm{Im}\left[\frac{-1}{\varepsilon(\mathrm{q},\omega)}\right] = \sum_{\mathrm{i}} \mathrm{A_i(q)}\mathrm{Im}\left[\frac{-1}{\varepsilon_{\mathrm{M}}(\mathrm{q},\omega,\ \omega_{\mathrm{i}},\ \Gamma_{\mathrm{i}})}\right]\Theta(\omega-\mathrm{E_{edge,i}}) \tag{5}$$

with

$$A_i(q) = A_i(0)\frac{\int_0^\infty d\omega\ \omega\ \mathrm{Im}\left[\frac{-1}{\varepsilon_{\mathrm{M}}(0,\omega,\omega_{\mathrm{i}},\Gamma_{\mathrm{i}})}\right]\Theta(\omega-\omega_{\mathrm{edge,i}})}{\int_0^\infty \mathrm{d}\omega\ \omega\ \mathrm{Im}\left[\frac{-1}{\varepsilon_{\mathrm{M}}(\mathrm{q},\omega,\omega_{\mathrm{i}},\Gamma_{\mathrm{i}})}\right]\Theta(\omega-\omega_{\mathrm{edge,i}})} \tag{6}$$

with $\Theta(x)$ the step function. In practice we determined $A_i(q)$ for q values at 0.1 a.u. interval and interpolated linearly to obtain $A_i(q)$ at any q value.

We compare both results with the loss function derived from the GOS adjusted so the edge is at the experimentally observed edge position, but scaled so the right number of electrons is obtained (the renormalized GOS method). For this purpose we study the cases of Al and Si and calculate various observables (proton stopping, electron inelastic mean free path, electron and proton induced L shell ionization, as well as the Compton profiles) for different ways of extending $\varepsilon(0, \omega)$ to q values $\neq 0$.

The method of Da et al. is an alternative way of fitting the sharp onsets of the semi-core ELF contribution as a sum of Mermin functions with both negative and positive A_i values [19,20]. Dielectric functions derived in this way automatically adhere to the sum rules at all q values and appear to describe the electron inelastic mean free path quite well. It would be of interest to study if a fit of the ELF with the method of Da et al. and the ones described here produce different values for $\mathrm{Im}[-1/\varepsilon(q, \omega)]$ away from $q = 0$, but this is beyond the topic of this paper.

For the calculation of all the observables described next only the knowledge of $\mathrm{Im}\left[\frac{-1}{\varepsilon(q,\omega)}\right]$ is required. As $\mathrm{Im}\ [1/\varepsilon(q, \omega)]$ and $\mathrm{Re}\ [1/\varepsilon(q, \omega)]$ are Kramers-Kronig pairs truncation of one or more Mermin oscillators, that together form $\mathrm{Im}\ [1/\varepsilon(q, \omega)]$, will affect $\mathrm{Re}\ [1/\varepsilon(q, \omega)]$, and hence $\mathrm{Re}\ [\varepsilon(q, \omega)]$ and $\mathrm{Im}\ [\varepsilon(q, \omega)]$ at all ω. After truncation or addition of a GOS to the dielectric function $\mathrm{Re}\ [\varepsilon(q, \omega)]$ and $\mathrm{Im}\ [\varepsilon(q, \omega)]$ cannot be derived any more directly from the Mermin dielectric function, but have to be retrieved by calculating $\mathrm{Re}\ [1/\varepsilon(q, \omega)]$, via a Kramer-Kronig transform.

3. Model dielectric function

3.1. Aluminum

For aluminum we used the ELF calculated from the dielectric

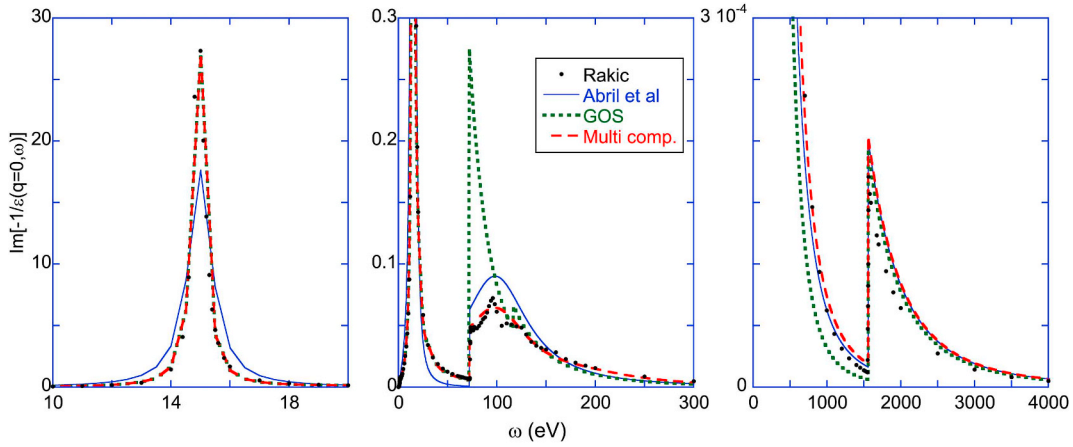

Fig. 2. The fit of the ELF of Al, based the optical data of Rakić [21] compared to several model dielectric function as explained in the main text.

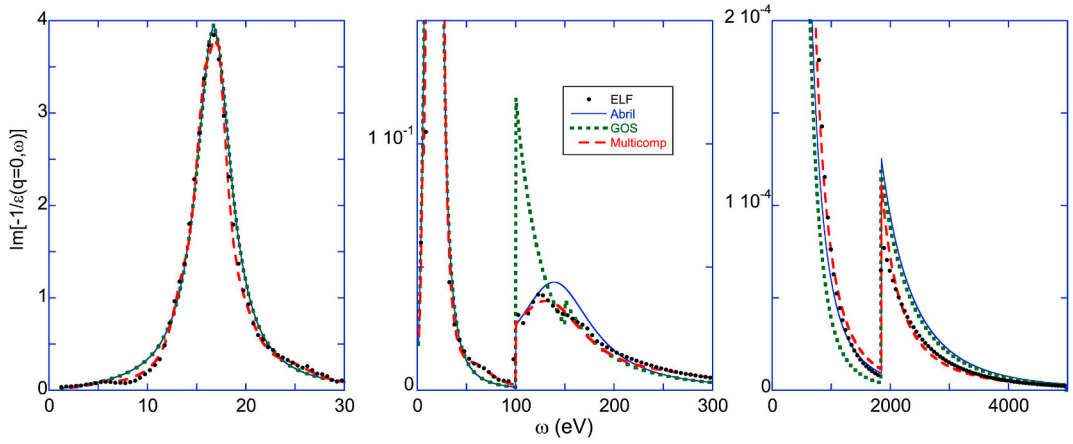

Fig. 3. The fit of the ELF of Si, based for low losses at the REELS work of Jin [22], and at large losses the tabulations of Henke [23].

constant as derived by Rakić [21] from different optical measurements covering together the complete range of energies of interest. It was derived in such a way that (among others) the Bethe sum rule, f sum rule and Kramers-Kronig relations were adhered to. Very similar results would be obtained using the data from the Palik handbook [5]. We compare it in Fig. 2 with the ELF corresponding to the dielectric function used by Abril et al. [12]. The latter has different shortcomings. The main plasmon component near 15 eV energy loss is too wide. Also the amplitude A_i of the valence band component is larger than 1 which is not in the spirit of the statistical approximation. In fact, this causes problems with the f-sum rule if $\varepsilon(q, \omega)$ is calculated via eq. (3). This problem has its roots in the fact that the calculated plasmon energy based on 3 electrons per atom (15.7 eV) is larger that the peak position of the measured energy loss distribution ($\approx$ 15 eV). Their L-loss feature starting near 100 eV is reasonably well in agreement with the ELF or Rakić. For the K electrons we use throughout the GOS in combination with the experimental 1s binding energy. Note that the vertical scale between the left and right plot differs by a factor 10^5. For the L shell we also calculated the GOS with the 2s and 2p contributions, again starting at the experimental 2s and 2p binding energies. The GOS was normalized such that the Bethe sum gave 2 and 6 electrons per atom for the 2s and 2p shell. The loss function obtained in this way, when compared to the Rakić ELF, is too high near the edge, and too low at larger energy losses.

To address some of these issues we did an empirical fit of the Rakić

Table 1
The parameters of the Al model dielectric function used here, and those used by Abril et all [12].

i	A_i	ω_1	Γ_i	ω_{edge}
1	0.904	14.95	0.46	–
2	0.022	19	6	–
3	0.011	54	80	–
4	0.007	31	15	–
5	0.007	22	5	–
6	0.002	17	1.5	–
7	0.044	106	82	72.5
8	0.005	200	140	72.5
ref. [12]				
1	1.1178	15	0.95	–
2	0.0666	106	82	72.5

Table 2
The parameters of the Si model dielectric function used here, and those used by Abril et all [12].

i	A_i	ω_i	Γ_i	ω_{edge}
1	0.015	5.5	2	–
2	0.1	13.5	2.5	–
3	0.29	15.7	2.2	–
4	0.39	17.2	2.3	–
5	0.068	20	4	–
6	0.035	25	6	–
7	0.004	65	40	–
8	0.024	100	140	99.8
9	0.0019	160	270	99.8
ref. [12]				
1	0.9922	16.8	4.24	–
2	0.05378	114	133	99.8

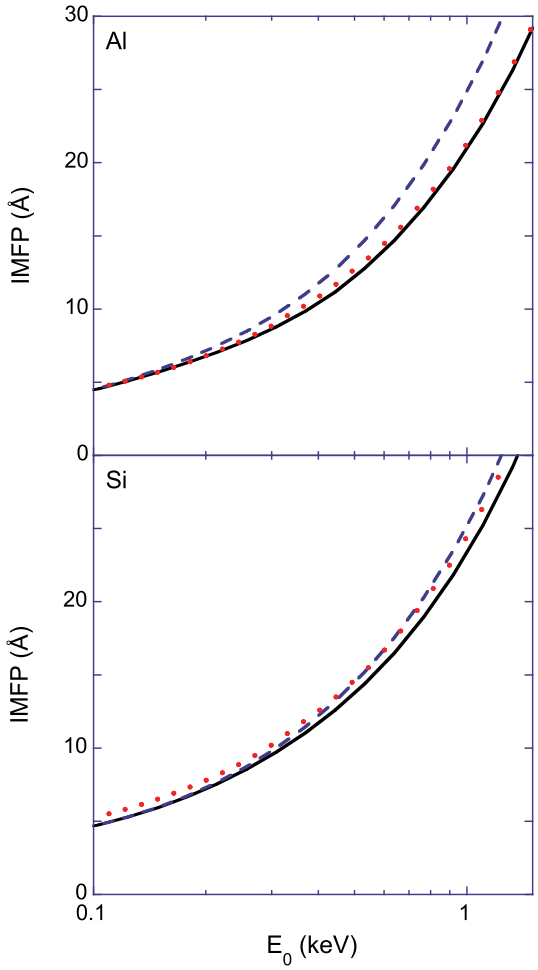

Fig. 4. The calculated electron inelastic mean free path for Al and Si based on the multi-component fit of the ELF, with (solid line) and without (dashed line) the contribution of the L shell. For comparison the values calculated by Tanuma et al. [25] using the full Penn model are shown as dots.

ELF using several Mermin components for the valence band and 2 truncated Mermin function for the L region, and again the GOS for the 1s level. By describing the main peak of the ELF, which is asymmetric, carefully with several components we can get for the valence band a good agreement with $\sum_{i=1}^{6} A_i = 0.953 < 1$, consistent with the statistical approximation. This value is less than 1 as a small fraction of space is occupied by the K and L electrons, the latter are presented by oscillators 7 and 8. As the data of Rakić are in agreement with the Bethe sum rule, the multi-component fit is in good agreement as well. The results are summarized in Table 1. The addition of more components improves, of course, the fit of the ELF considerably, but we want to investigate to what extent a more accurate description of the ELF results in a better description of observables such as ion stopping and ionization probabilities.

3.2. Silicon

For Silicon we obtained an estimate of the ELF by combining the ELF at $q = 0$ from Jin et al. [22] for low energy losses (up to 50 eV), obtained using reflection electron energy loss spectroscopy, with the one calculated from the optical data of Henke [23], see Fig. 3. Both data sets connect smoothly. The same fitting approaches are used as for Al (Table 2). For the multi-component fit it was checked that the refractive index for Si near $\omega = 0$ corresponds to the literature value of 11.6 (which requires that $\sum_i A_i < 1$ for the A_i modelling the valence band [24]).

4. Electron inelastic mean free path

For completeness we start by comparing the inelastic mean free path (IMFP or λ) for electrons with energy E_0 with those obtained from the full-Penn algorithm, generally considered the best estimate available of this quantity [25,26]. The IMFP is calculated using:

$$1/\lambda = \int_0^{E_0-E_f} \frac{d\omega}{\pi E_0} \int_{q_-}^{q_+} \frac{dq}{q} \mathrm{Im}\left[\frac{-1}{\varepsilon(q,\omega)}\right]$$

$$= \int_0^{E_0-E_f} \frac{2d\omega}{\pi v^2} \int_{q_-}^{q_+} \frac{dq}{q} \mathrm{Im}\left[\frac{-1}{\varepsilon(q,\omega)}\right] \quad (7)$$

with v the projectile velocity, E_f the Fermi energy and

$$q_\pm = \sqrt{2ME_0} \pm \sqrt{2M(E_0-\omega)}\,. \quad (8)$$

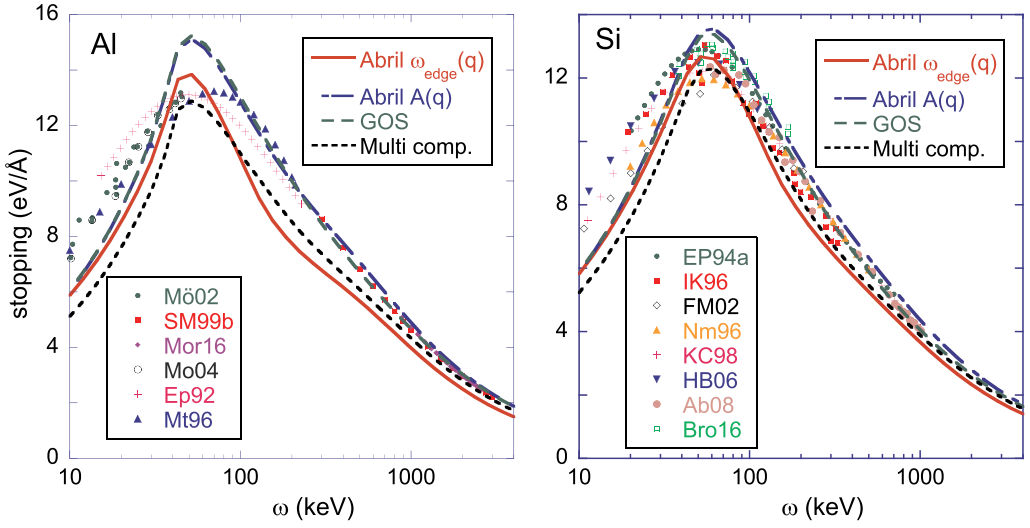

Fig. 5. The calculated stopping, for the various models as discussed in the main text for Al and Si. The experimental points are from post-1990 experiments, taken from https://www-nds.iaea.org/stopping/.

with M the projectile (electron) mass.

The comparison is shown in Fig. 4. For Al we find very good agreement but for Si the IMFP obtained here is about 6% smaller than that obtained by the full Penn Algorithm [25]. De la Cruz and Yubero analyzed the IMFP of Si in a similar way and also obtained an IMFP for Si that was slightly too small [27].

The contribution of the L shell to the IMFP is small, but significant. It is larger for Al, as the L binding energies are for Al less than for Si. However, differences of the mentioned extension models for the L level causes variations of the IMFP only on a 1% level, too small to reach any conclusion, when comparing with experiments.

5. Stopping

Another quantity often derived from the dielectric function is the ion stopping power. The simplest case for protons will be considered here and for energies larger than 100 keV it is a very good approximation to consider the protons fully ionized. The ion stopping power is determined from the induced retarding force at the ion position and therefore from the dielectric function according to

$$\frac{dE}{dx} = \frac{2}{\pi v^2}\int_0^{\infty}\frac{dq}{q}\int_0^{qv}\omega\, d\omega\ \mathrm{Im}\left[\frac{-1}{\varepsilon(q,\omega)}\right]. \tag{9}$$

In addition by changing the order of integration we can change this equation to

$$\frac{dE}{dx} = \int_0^{E_0}\frac{2\omega\, d\omega}{\pi v^2}\int_{q_-}^{q_+}\frac{dq}{q}\ \mathrm{Im}\left[\frac{-1}{\varepsilon(q,\omega)}\right], \tag{10}$$

which is more similar to Eq. (7). Here v is now the proton velocity and the $q_{\pm}$ limits are again calculated using eq. (8), but now of course using the proton mass. eq. (10) highlights the similarity with the IMFP calculation, but now the contribution of each inelastic event is weighted by the corresponding energy loss ω. Hence the contribution of the L levels is more pronounced for proton stopping than for the electron IMFP.

As is clear in Fig. 5 (left panel) the calculation of ref. [12], labelled 'Abril ω_{edge}' using *their* parameters and a truncation energy that changes with q, reproduced the general shape of the Al stopping curve quite well, but the calculated stopping value were slightly too low, especially for $E > 100$ keV. The agreement improves if we use the *same* model parameters, with a single truncation energy but with $A(q)$ varied in such a way that the sum rule is fulfilled (curve labelled 'Abril $A(q)$'). The calculation of the stopping using the GOS approach for the L shell, normalized to the nominal number of electrons in the shell is very close to the $A(q)$ values. If we use the multi-component fit of Table 1 in conjunction with the $A(q)$ method than the stopping reduces somewhat, but remains above that calculated in Ref. [12]. Using the multi-component fit in conjunction with the $\omega_{edge}(q)$ method provides even smaller stopping powers than those calculated by Abril et al. [12]. For energies below 100 keV the experimental stopping is lower than all calculated values, due to non-linear effects for the Al valence band electrons that come into play at lower projectile energies [28,29].

The Si results shown in Fig. 5 (right panel) are very similar, except that the influence of the L shell is slightly less, as its binding energy increases with Z.

6. Proton and electron-induced excitation

The sharp onsets in the ELF near 72.5 eV (Al) and 100 eV (Si) are related to excitation of the L shell electrons. Hence by integrating eq. (7) but considering only the truncated Mermin part of the ELF (or GOS part), one should get an estimate of the L shell ionization probability per unit length travelled. Identifying the contribution from inner-shell ionization is also important for micro- and nano-dosimetry in medical physics [30]. These calculations were done for the Al case for both electrons and protons. The results are displayed in Fig. 6. Clearly the ionization probability depends strongly on the way the dielectric function is extended to finite q values. The $\omega_{edge}(q)$ method requires a larger projectile energy for the ionization to happen and results in smaller cross sections. For electrons we can compare our cross section with those calculated using the (*atomic*) distorted wave calculation from LLovet et al. [31,32]. These calculations do not predict a delayed onset of the ionization, but a shape of the ionization probability rather similar to the $A(q)$ method or when using a GOS to describe these levels. The GOS (in particular if one does not re-normalize the GOS in such a way that it gives the right Bethe sum) cross sections are considerable larger than those obtained by the $A(q)$ method. If one replaces the single truncated Mermin, from Ref. [12] with 2 truncated Mermins, as in the multicomponent fit, then one obtains a surprisingly good agreement with the calculation of LLovet et al.

For proton ionization the increased threshold of the ionization process for the $\omega_{edge}(q)$ method is even more obvious. Here we have experimental evidence from the LVV Auger yield measurement of Lee and Pfandzelter [33], as the L Auger yield should mirror the ionization probability. The Auger yield increases strongly for proton energies above 10 keV, much earlier than the threshold predicted by the $\omega_{edge}(q)$ method. Again the GOS theory without renormalization gives the largest cross section which is very similar to the one calculated by the ECPSSR program [34] used for PIXE measurements, suggesting that the ECPSSR program does not use the Bethe sum rule to renormalize their GOS. These L levels are however, at too low an energy to be of use in PIXE experiments, and in the PIXE energy range a GOS-based description, without additional normalization should be sufficiently accurate.

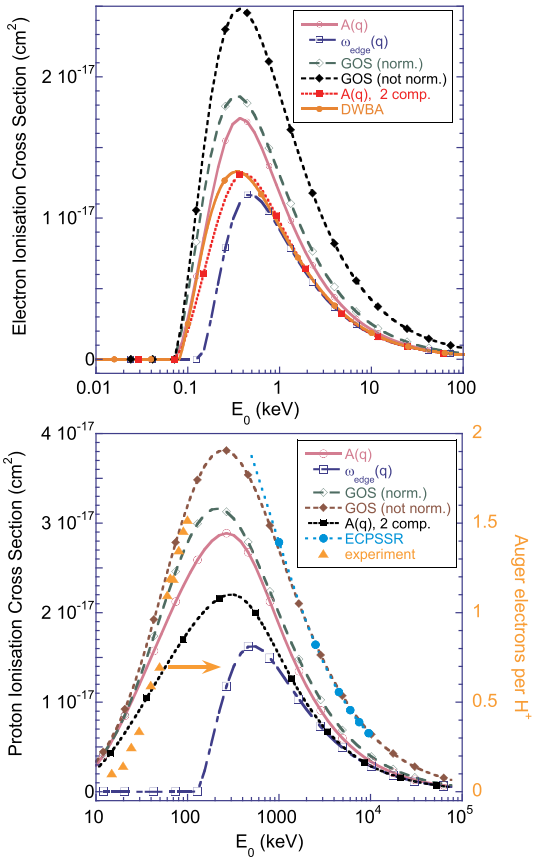

Fig. 6. The L shell ionization for Al induced by electrons (top) and protons (bottom) for the various models compared to Distorted-wave Born approximation (DWBA) (top) and compared to ECPSSR calulations and measured Auger yields (bottom).

7. Compton profile

Now we will investigate if any of the extension methods described here give a good description in the high-q limit. At high q the projectile interacts with a single target electron only. The energy transfer is in that case large, much larger than the binding energy of the electron and the collision can be described in terms of a collision of the projectile with a free electron. If this electron has momentum p before the collision then the energy-transfer to the electron E_{recoil} (and hence the energy loss ω of the projectile) is equal to [35].

$$E_{\text{recoil}} = \frac{q^2}{2} + \mathbf{p}\cdot\mathbf{q} \tag{11}$$

The energy loss distribution can then be plotted as a Compton profile (i.e. the number of electrons with a certain amount of momentum along $\mathbf{q}$: (p_q)) by changing the energy loss scale into a momentum scale according to [35]:

$$p_q = \frac{(\omega - q^2/2)}{q} \tag{12}$$

The dielectric function was calculated for $q = 30$ a.u. and is shown in Fig. 7 both as a function of ω and p_q as calculated via eq. (12). It is compared with an experimental Compton profile obtained using X-ray scattering. The valence electrons contribute roughly between -1 and 1 a.u. The L-shell electrons contribute over a larger range for momenta, between -4 and 4 a.u. The K shell contribution extends to even larger momenta. The area corresponding to the valence, L and K shell is proportional to the number of electrons occupying it i.e. for Si 4:8:2.

The $\omega_{\text{edge}}(q)$ method (not developed for these conditions) causes a large asymmetry in the Compton profile, as it is truncated at the low-energy loss side in order to correspond to the same number of electrons as at $q = 0$. The $A(q)$ method approaches the Compton profile somewhat better, in particular if the multicomponent fit of the ELF is used. Finally, the multi-component fit of the valence band in combination with the use of a (normalized) GOS description of the L level describes the experimental Compton profile surprisingly well.

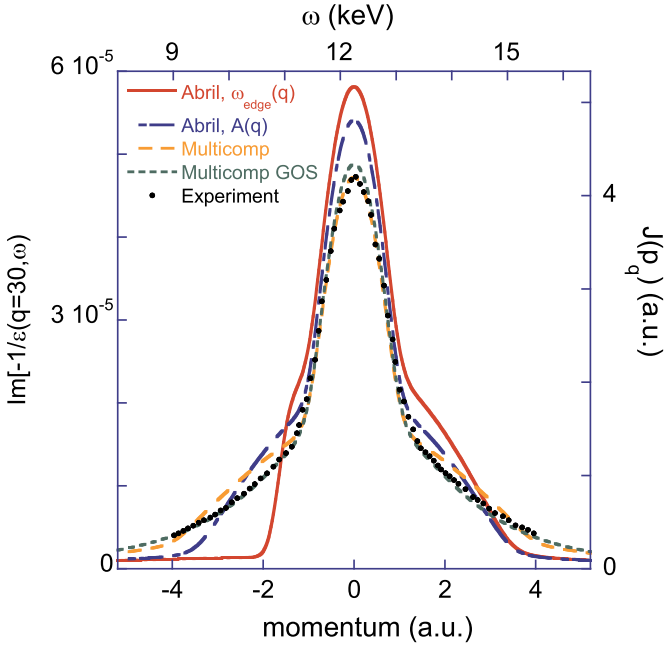

Fig. 7. The calculated Compton profile for the various models as indicated, calculated for $q = 30$ a.u. compared to the experimental data [36]. The calculated Compton profile are broadened by the experimental resolution (0.45 a.u.).

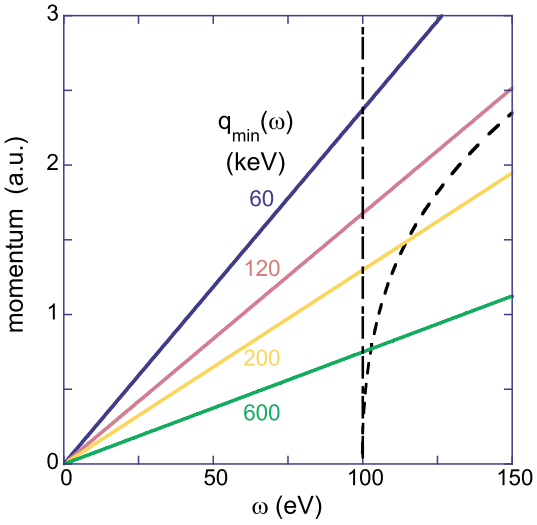

Fig. 8. The dependence of the q_{min} on ω and the position of the Si L edge in the $A(q)$ (vertical line) and $\omega_{\text{edge}}(q)$ model (parabola-like line).

8. Discussion

Finally we want to explain why the $\omega_{\text{edge}}(q)$ method results in an underestimation of the stopping power and ionization cross section, as well as the increased projectile energy threshold for ionization that is predicted by this approach.

Energy loss of the projectile means a reduction of its momentum, and hence there is a momentum transfer q, even if the direction of propagation does not change. This minimum momentum transfer is given by q_- in eq. (8). For a certain ω value q_- decreases if the projectile energy increases. In Fig. 8 we plot q_- for various proton energies as a function of ω (a qualitatively similar picture would apply to electrons). In this plot we also indicated the energy where the Mermin function is truncated for Si: a vertical line for the $A(q)$ method and a curved line for the ω_{edge} method. Take, as an example, the 60 keV proton case. It crosses the $A(q)$ truncation line for $q \approx 2.3$ a.u. Thus the momentum transfer for an L level excitation by a 60 keV proton is *at least* 2.3 a.u. Note also that for 60 keV the q_- line never crosses the $\omega_{\text{edge}}(q)$ truncation line. This means that, within that approach, a 60 keV proton cannot excite an L shell electron, and hence these electrons will not contribute to the proton stopping. For the proton to be able to excite an L-shell electron in the $\omega_{\text{edge}}(q)$ model it needs at least ≈140 keV energy. Even if the threshold is reached its contribution to the stopping will remain smaller as the accessible phase space is less and all the contributions to the stopping (eq. (10)) correspond to larger q values (which is in the denominator of eq. (10)).

A different way of getting insight in these matters is by plotting $\text{Im}[-1/\varepsilon(q, \omega)]$ but only for the part of the phase space that is accessible. (note that to determine the contribution to e.g. the inelastic mean free path (eq. (7)) or stopping (eq. (10)) one still has to divide $\text{Im}[-1/\varepsilon(q, \omega)]$ by q) For Al this is done in Fig. 9 for both protons and electrons, at the energies as indicated. The intensity plotted is for the $A(q)$ model but the dashed line shows the position of the edge in the $\omega_{\text{edge}}(q)$ approach. For electrons the accessible space extends to where the energy loss is equal to the projectile energy. The boundary at the left (smaller q values) of this point is due to q_-, the boundary at the right due to q_+ (see eq. (8)). For 20 eV electrons the plasmon does not contribute, and all intensity is due to electron-hole pair excitation. At 80 eV both the plasmon and the electron-hole brach of the excitation spectrum contributes, and even the L shell corresponds a little in the $A(q)$ model, but not in the $\omega_{\text{edge}}(q)$ model (as the dashed line is not crossed. At 200 eV the L level starts contributing as well in the $\omega_{\text{edge}}(q)$ model.

For protons the situation is somewhat different. At 20 keV the

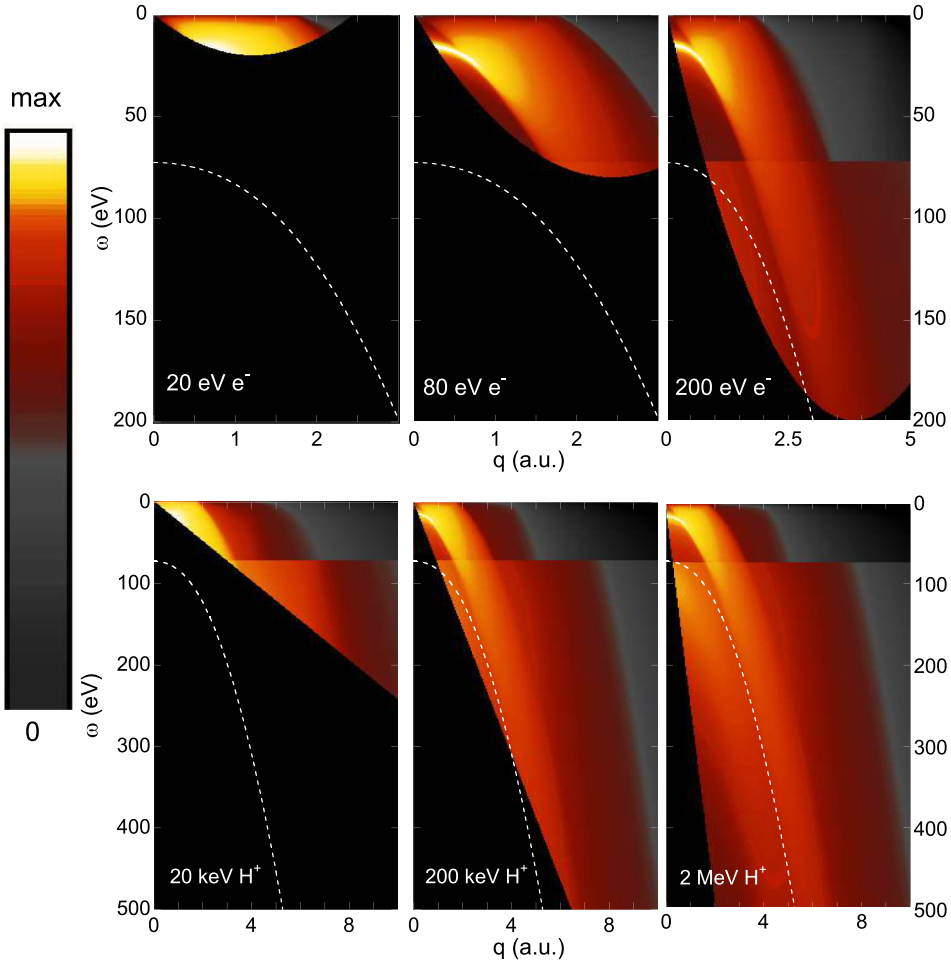

Fig. 9. Color plot of $\log(\mathrm{Im}[-1/\varepsilon(q,\omega)])$ of the dielectric function of Al for the fraction of (q, ω) space that is accessible for the electrons (top) and protons (bottom) for the projectile energy as indicated (see eq. (8)). The dashed line shows the L edge in the $\omega_{\mathrm{edge}}(q)$ model. (The log was taken to make both the low-intensity and high-intensity features clearly visible. Each panel is independently normalized so the maximum intensity corresponds to white.). (For interpretation of the references to colour in this figure legend, the reader is referred to the Web version of this article.)

energy loss excitations are mainly in the electron-hole branch but it is possible to excite an L electron at relatively large momentum (≈ 4 a.u.) in the $A(q)$ model but not in the $\omega_{\mathrm{edge}}(q)$ approach. At 200 keV the plasmon contribution dominates, and the L electrons just start contributing in the $\omega_{\mathrm{edge}}(q)$ model and only for energy losses <300 eV (where the dashed line crosses the q_{min} boundary for a second time). At 2 MeV the excitation spectrum of the L electrons extend to much larger energies.

Recently the use of the MLL (Mermin-Levine-Louie) dielectric function was suggested [24] for the description of the dielectric function of insulators, i.e. the Levine-Louie dielectric function [37] modified by a relaxation time [38]. Here a band gap (magnitude U) is incorporated in the model that shifts the intensity of the loss function to larger values. For $q = 0$ the ELF retains a Lorentzian shape but the peak position shifts from ω_i to $\sqrt{(\omega_i^2 + U^2)}$. For $q \neq 0$ the intensity for $\omega < U$ is strongly reduced compared to the Mermin loss function peaking at $q = 0$ at the same ω value. One could be tempted to use a similar approach for the semicore levels, modelling the binding energy in some way by the U parameter, but the fitting of the discontinuity of the ELF at the edge would be as difficult with an MLL approach as with the Mermin approach.

9. Conclusion

We calculated several observables related to the dielectric function and compared the outcome with experimental results, where available. In general the best results were obtained when using an accurate fit of the ELF based on a sum of Mermin dielectric functions, with those representing outer core electrons truncated. Extension of the dielectric function to all q values it then best done by taking the magnitude of the truncated Mermin contribution to be a function of q in such a way that the Bethe sum rule is fulfilled. In this way one can describe the ion stopping, ionization probabilities and Compton profile reasonably well.

References

[1] M. Dapor, Transport of Energetic Electrons in Solids: Computer Simulation with Applications to Materials Analysis and Characterization, Springer Tracts in Modern Physics.
[2] H. Nikjoo, S. Uehara, D. Emfietzoglou, Interaction of Radiation with Matter, CRC press, 2012.
[3] R.H. Ritchie, Plasma losses by fast electrons in thin films, Phys. Rev. 106 (1957) 874–881, https://doi.org/10.1103/PhysRev.106.874.
[4] P. Sigmund, Particle Penetration and Radiation Effects, Vol. 151 of Springer Series in Solid-state Sciences, Springer, Berlin, 2006.
[5] E. Palik, Handbook of Optical Constants of Solids II, Academic Press, New York, 1991.
[6] D. Emfietzoglou, R. Garcia-Molina, I. Kyriakou, I. Abril, H. Nikjoo, A dielectric response study of the electronic stopping power of liquid water for energetic protons and a newI-value for water, Phys. Med. Biol. 54 (2009) 3451, https://doi.org/10.1088/0031-9155/54/11/012.
[7] S. Tanuma, C. Powell, D. Penn, Use of sum rules on the energy-loss function for the evaluation of experimental optical data, J. Electron. Spectrosc. Relat. Phenom. 62 (1993) 95, https://doi.org/10.1016/0368-2048(93)80008-a.
[8] F. Yubero, S. Tougaard, Quantitative analysis of reflection electron energy-loss spectra, Surf. Interface Anal. 19 (1992) 269–273, https://doi.org/10.1002/sia.

740190152.
[9] N. Medvedev, R. Rymzhanov, A. Volkov, Time-resolved electron kinetics in swift heavy ion irradiated solids, J. Phys. Appl. Phys. 48 (2015) 355303, https://doi.org/10.1088/0022-3727/48/35/355303.
[10] R. Rymzhanov, N. Medvedev, A. Volkov, Effects of model approximations for electron, hole, and photon transport in swift heavy ion tracks, Nucl. Instrum. Methods Phys. Res. Sect. B Beam Interact. Mater. Atoms 388 (2016) 41, https://doi.org/10.1016/j.nimb.2016.11.002.
[11] D. Penn, Electron mean-free-path calculations using a model dielectric function, Phys. Rev. B 35 (1987) 482–486, https://doi.org/10.1103/PhysRevB.35.482.
[12] I. Abril, R. Garcia-Molina, C. Denton, F. Pérez-Pérez, N. Arista, Dielectric description of wakes and stopping powers in solids, Phys. Rev. A 58 (1998) 357, https://doi.org/10.1103/physreva.58.357.
[13] H. Nikjoo, D. Emfietzoglou, T. Liamsuwan, R. Taleei, D. Liljequist, S. Uehara, Radiation track, DNA damage and response—a review, Rep. Prog. Phys. 79 (2016) 116601, https://doi.org/10.1088/0034-4885/79/11/116601.
[14] R.H. Ritchie, A. Howie, Electron excitation and the optical potential in electron microscopy, Philos. Mag. A 36 (1977) 463, https://doi.org/10.1080/14786437708244948.
[15] C. Tung, J. Ashley, R. Ritchie, Electron inelastic mean free paths and energy losses in solids ii: electron gas statistical model, Surf. Sci. 81 (2) (1979) 427, https://doi.org/10.1016/0039-6028(79)90110-9.
[16] J.C. Slater, Atomic shielding constants, Phys. Rev. 36 (1930) 57, https://doi.org/10.1103/physrev.36.57.
[17] R.F. Egerton, Electron Energy-loss Spectroscopy in the Electron Microscope, Plenum Press, New York, 1996.
[18] X-ray data booklet (http://xdb.lbl.gov/).
[19] B. Da, H. Shinotsuka, H. Yoshikawa, Z.J. Ding, S. Tanuma, Extended Mermin method for calculating the electron inelastic mean free path, Phys. Rev. Lett. 113 (2014) 063201, , https://doi.org/10.1103/physrevlett.113.063201.
[20] Y. Sun, H. Xu, B. Da, S. feng Mao, Z. jun Ding, Calculations of energy-loss function for 26 materials, Chin. J. Chem. Phys. 29 (2016) 663, https://doi.org/10.1063/1674-0068/29/cjcp1605110.
[21] A.D. Rakić, Algorithm for the determination of intrinsic optical constants of metal films: application to aluminum, Appl. Optic. 34 (1995) 4755, https://doi.org/10.1364/ao.34.004755.
[22] H. Jin, H. Shinotsuka, H. Yoshikawa, H. Iwai, S. Tanuma, S. Tougaard, Measurement of optical constants of Si and SiO_2 from reflection electron energy loss spectra using factor analysis method, J. Appl. Phys. 107 (2010) 083709, , https://doi.org/10.1063/1.3346345.
[23] B. Henke, E. Gullikson, J. Davis, X-ray interactions: photoabsorption, scattering, transmission, and reflection at e = 50-30,000 eV, z = 1-92, Atomic Data Nucl. Data Tables 54 (1993) 181, https://doi.org/10.1006/adnd.1993.1013.
[24] M. Vos, P. Grande, Simple model dielectric functions for insulators, J. Phys. Chem. Solid. 104 (2017) 192, https://doi.org/10.1016/j.jpcs.2016.12.015.
[25] S. Tanuma, C.J. Powell, D.R. Penn, Calculations of electron inelastic mean free paths. IX. Data for 41 elemental solids over the 50 eV to 30 keV range, Surf. Interface Anal. 43 (2011) 689, https://doi.org/10.1002/sia.3522.
[26] H. Shinotsuka, S. Tanuma, C.J. Powell, D.R. Penn, Calculations of electron inelastic mean free paths. X. Data for 41 elemental solids over the 50 eV to 200 keV range with the relativistic full Penn algorithm, Surf. Interface Anal. 47 (2015) 871, https://doi.org/10.1002/sia.5789.
[27] W. de la Cruz, F. Yubero, Electron inelastic mean free paths: influence of the modelling energy-loss function, Surf. Interface Anal. 39 (2007) 460, https://doi.org/10.1002/sia.2545.
[28] D. Primetzhofer, S. Rund, D. Roth, D. Goebl, P. Bauer, Electronic excitations of slow ions in a free electron gas metal: evidence for charge exchange effects, Phys. Rev. Lett. 107, http://doi.dx.org.10.1103/physrevlett.107.163201.
[29] P. L. Grande, Alternative treatment for the energy-transfer and transport cross section in dressed electron-ion binary collisions, Phys. Rev. A 94, http://doi.dx.org.10.1103/physreva.94.042704.
[30] I. Kyriakou, S. Incerti, Z. Francis, Technical note: improvements in Geant4 energy-loss model and the effect on low-energy electron transport in liquid water, Med. Phys. 42 (2015) 38706, https://doi.org/10.1118/1.4921613.
[31] X. Llovet, C.J. Powell, F. Salvat, A. Jablonski, Cross sections for inner-shell ionization by electron impact, J. Phys. Chem. Ref. Data 43 (2014) 013102, , https://doi.org/10.1063/1.4832851.
[32] D. Bote, F. Salvat, A. Jablonski, C.J. Powell, Cross sections for ionization of K, L and M shells of atoms by impact of electrons and positrons with energies up to 1GeV: analytical formulas, Atomic Data Nucl. Data Tables 95 (2009) 871, https://doi.org/10.1016/j.adt.2009.08.001.
[33] J. Lee, R. Pfandzelter, Si L23VV auger electron emission induced by specularly reflected protons, Surf. Sci. 225 (1990) 301, https://doi.org/10.1016/0039-6028(90)90451-d.
[34] W. Brandt, G. Lapicki, Energy-loss effect in inner-shell Coulomb ionization by heavy charged particles, Phys. Rev. A 23 (1981) 1717, https://doi.org/10.1103/physreva.23.1717.
[35] M. Vos, A model dielectric function for low and very high momentum transfer, Nucl. Instrum. Methods Phys. Res., Sect. B 366 (2015) 6, https://doi.org/10.1016/j.nimb.2015.09.091.
[36] J.S. Tse, D.D. Klug, D.T. Jiang, C. Sternemann, M. Volmer, S. Huotari, N. Hiraoka, V. Honkimki, K. Hmlinen, Compton scattering of elemental silicon at high pressure, Appl. Phys. Lett. 87 (2005) 191905, https://doi.org/10.1063/1.2126125.
[37] Z. Levine, S. Louie, New model dielectric function and exchange-correlation potential for semiconductors and insulators, Phys. Rev. B 25 (1982) 6310, https://doi.org/10.1103/physrevb.25.6310.
[38] N. Mermin, Lindhard dielectric function in the relaxation-time approximation, Phys. Rev. B 1 (1970) 2362–2363, https://doi.org/10.1103/physrevb.1.2362.